Wiley
Nanomaterials and Nanotechnology
Volume 2025, Article ID 4276075, 12 pages
https://doi.org/10.1155/nax2/4276075

Research Article

Green Synthesis of Pure and Zirconium-Doped Cerium Oxide Nanoparticles Using Aqueous Extract of *Sanvitalia procumbens*, Its Characterization, Antiplatelet and Cytotoxic Activities

Tasmeena Parveen,[1] Ijaz Ahmad ,[1] Madeeha Aslam,[1] Fozia Fozia ,[2] Ahmad Khushal,[3] Mohamed Mohany ,[4] Salim S. Al-Rejaie ,[4] Ziaullah Ziaullah ,[5] and Marija Milošević [6]

[1]*Department of Chemistry, Kohat University of Science & Technology, Kohat 26000, Pakistan*
[2]*Department of Biochemistry, Khyber Medical University Institute of Dental Sciences, Kohat 26000, Pakistan*
[3]*Department of Medicine and Surgery, Khyber Medical College, Peshawar 25120, Khyber-Pakhtunkhwa, Pakistan*
[4]*Department of Pharmacology and Toxicology, College of Pharmacy, King Saud University, P.O. Box 55760, Riyadh 11451, Saudi Arabia*
[5]*Department of Biological Sciences, College of Professional Studies, Northeastern University, Boston, Massachusetts, USA*
[6]*Department of Biology and Ecology, Faculty of Science, University of Kragujevac 34000, Kragujevac, Serbia*

Correspondence should be addressed to Ijaz Ahmad; drijaz_chem@yahoo.com and Fozia Fozia; drfoziazeb@yahoo.com

Received 27 June 2024; Accepted 20 December 2024

Academic Editor: Leander Tapfer

Copyright © 2025 Tasmeena Parveen et al. Nanomaterials and Nanotechnology published by John Wiley & Sons Ltd. This is an open access article under the terms of the Creative Commons Attribution License, which permits use, distribution and reproduction in any medium, provided the original work is properly cited.

The current study was used to achieved the green synthesis of pure with different percentages of zirconium-doped cerium oxide nanoparticles (Zr-doped CeO_2 NPs) using an aqueous plant extract of *Sanvitalia procumbens*. The synthesis of pure NPs was achieved by mixing 30 mL of Ce $(NO_3)_3{\cdot}6H_2O$ into 10 mL of plant extract and then adding ZrO $(NO_3)_2$. xH_2O into a reaction mixture to synthesize Zr-doped CeO_2 NPs with the variation of x ($x = 5\%$, 10%, and 15%). The phytochemicals present in *Sanvitalia procumbens* plant extract function as stabilizing and reducing agent which may have ability to synthesize pure and Zr-doped CeO_2 NPs. The synthesized NPs were characterized by different analytical techniques, such as UV-visible (UV-Vis), scanning electron microscopy (SEM), energy dispersive X-ray (EDX), Fourier transform infrared spectroscopy (FT-IR), and powder X-ray diffraction (PXRD). The UV-Vis spectroscopy revealed that zirconium (Zr) was well doped in CeO_2 NPs with a band gap energy of 4.07–4.56 eV. The SEM images demonstrate the irregular morphology with an average particle size range of 26.72, 24.37, 21.24, and 19.12 nm for pure, 5%, 10%, and 15% Zr-doped CeO_2 NPs, respectively. The fundamental elemental composition of Zr-doped CeO_2 NPs was ascertained by EDX analysis, whereas the PXRD patterns support the crystalline nature of NPs. Furthermore, the synthesized pure and Zr-doped CeO_2 NPs were used to analyze the antiplatelet activity that showed dose-dependent antiplatelet potentials. The results revealed that 15% Zr-doped CeO_2 NPs showed maximum antiplatelet activity that was 84.24 s at concentrations of 100 μg/mL. Moreover, the IMR32 cell line was also studied to demonstrate the cytotoxicity of pure and Zr-doped CeO_2 NPs. Accordingly, Zr-doped CeO_2 NPs exhibits higher cytotoxic effects against brain cancer in contrast to undoped CeO_2 NPs. Thus, the obtained results suggest the potential use of Zr-doped CeO_2 NPs as an industrial application such as in the development of antiplatelet and cytotoxic activity.

Keywords: antiplatelet; cytotoxic activities; green synthesis; pure and Zr-doped CeO_2 NPs; *Sanvitalia procumbens*

1. Introduction

Cerium oxide nanoparticles (CeO_2 NPs) are considered as oxide of a rare earth metal that have cubic fluorite crystal structure and can exhibit different physical and chemical properties [1]. Owing to its significant characteristics, CeO_2 NPs have been used in different biomedical fields, including sensors, solid oxide fuel cells, catalysts, sunscreen, potent antioxidants, and antibacterial activities [2]. Furthermore, the reactivity and stability of CeO_2 NPs increase by doping with different metals such as, Ag, Sn, Zr, and Cu for different medical fields. It has been observed that Zr-doped CeO_2 is highly effective than other dopants [3]. Hence, the combination of Zr and cerium core metal oxide NPs (ZrO_2/CeO_2) has high thermal stability, large surfaces, excellent oxygen storage capability, and significant redox characteristics [4]. Furthermore, the inclusion of Zr ions into the crystal structure of CeO_2 generates an alteration in the lattice structure of the cubic fluorite and enhanced the number of oxygen vacancy. The redox reaction permits the influx of Ce^{3+} and Ce^{4+}, which increase the rate of the catalytic reaction and facilitate product desorption on the catalyst [5, 6]. The substantial effect on their efficiency and on size of the NPs was observed when Zr ions are doped into high surface area of CeO_2 NPs. Thus, the incorporation of Zr dopant is an efficient procedure that enhanced the biological potential of CeO_2 NPs. Moreover, different methods have been used to synthesize CeO_2 NPs and Zr-doped CeO_2 NPs that include the sol–gel method [7], hydrothermal method [8], co-precipitation [9], and solid-state template method [10]. Majority of these physical and chemical methods require the use of hazardous materials and high-reaction conditions that are an expensive and complex for the synthesis of NPs which may cause environmental contamination and chemical toxicity. However, green synthesis includes actinomycetes, bacteria, fungi, and algae which use dispersants and end-capping agents that require high energy and may involve the use of toxic and harmful reagents [11]. Therefore, the plant-mediated green synthesis of CeO_2 NPs was demonstrated as an environmentally safe, cost-effective, and nontoxic method that minimized the band gap energy and improved the characteristics of the final product of the reaction mixture [12]. Recently, CeO_2 NPs were efficiently fabricated by using an aqueous plant extract including *Acalypha indica* [2], *Olea europaea* [13], and *Jatropha curcas* [14].

Thus, plant extracts have been successfully used in the green synthesis of Zr-doped CeO_2 NPs and exhibit promising biological properties like antibiofilm, antibacterial, and antioxidant activity [15]. CeO_2 NPs are distinct Ce^{4+} sites that are responsible for catalase mimetic oxidation of H_2O_2, whereas the superoxide dismutase mimetics are considered to be primarily responsible for the removal of $^{\cdot}OH$ and O_2^- through redox reactions. So, both $^{\cdot}OH$ and O^{2-} are directly associated with inflammatory response and cell death [16, 17]. Hence, the catalytic performance of CeO_2 NPs in scavenging reactive oxygen species (ROS) generation is influenced by the addition of Zr^{4+} ions. Thus, Zr-doped CeO_2 NPs also exhibit antiplatelet and cytotoxic activities that are indicated by their properties that can be altered by doping of CeO_2 NPs. The demand for new drugs with potent antiplatelet activity without negative side effects is increasing due to the significant impact of platelets on hemostasis and thrombosis. Although platelets are essential for numerous physiological processes, their excessive activity can lead to several health issues, including a risk of death from complications in biological systems [18]. Heart failure has been well-characterized in terms of platelet abnormalities. Both acute and chronic stages of cardiovascular disorders are influenced by the dysfunction of platelets. Thus, the use of antiplatelet medications has become increasingly important in combating various disorders affecting the cerebral, peripheral artery, and cardiovascular systems [19]. Blood thinners such as heparin, aspirin, and many more are used to treat such ailments, but synthetic medications may cause certain unfavorable side effects [20]. Similarly, previous research indicates that consuming aspirin at a dose of 0.4%–35% fails to result in adequate antiplatelet activity and raises the risk of cardiovascular illnesses [21]. So, medicinal plants are rich in bioactive compounds that reduce platelet activity, so it might be beneficial to prevent platelet aggregation. Therefore, plant-mediated pure and Zr-doped CeO_2 NPs synthesis remains one of the most potent alternatives for therapeutic purposes and hence can be detected as a key source for antiplatelet drug.

Furthermore, the CeO_2 NPs and Zr-doped CeO_2 NPs synthesis was previously reported by using an aqueous extract of different plants and was also reported for different biological activities [5, 6, 9]. Thus, there is no specific literature available on green source synthesis of pure and Zr-doped CeO_2 NPs utilizing *Sanvitalia procumbens* an aqueous plant extract. So, this work reports green source fabrication of pure with different percentage of Zr-doped CeO_2 NPs using plant extract of *Sanvitalia procumbens*. The perpetual flowering ornamental plant *Sanvitalia procumbens* is widely grown around the world and belongs to the member of the Asteraceae (sunflower) family. The species *Sanvitalia procumbens* are New World being limited in distribution to Arizona and New Mexico in the north, western Texas in the east, Central America in the south, and Mexico in the west. The foliar features of *Sanvitalia procumbens* are extremely diverse that are used for indigestion, dysentery, respiratory afflictions, and diarrhea, and the leaf extract is used as an appetizer [22, 23]. Moreover, the plant extract contains essential phytochemicals, including phenolics, terpenoids, proteins, galuteolin, quercetin, 3, 5-O-caffeoylquinic acid, chlorogenic acid, and alkamides. These phytochemicals may serve as reducing and stabilizing agents for the synthesis of pure and Zr-doped CeO_2 NPs [24]. In addition, the green synthesized pure, 5%, 10%, and 15% Zr-doped CeO_2 NPs from *Sanvitalia procumbens* plant extract were analyzed by different characterization techniques including UV-visible (UV-Vis), Fourier transform infrared spectroscopy (FT-IR), scanning electron microscopy (SEM), powder X-ray diffraction (PXRD), and energy dispersive X-ray (EDX) analysis. Furthermore, the current study

reports the MTT assay that is used for the first time to evaluate the biological application in terms of their antiplatelet and cytotoxic activities using green synthesized pure, 5%, 10%, and 15% Zr-doped CeO_2 NPs.

2. Materials and Methods

2.1. Plant Extraction. The fresh plant *Sanvitalia procumbens* was collected from KDA, Kohat, Pakistan. The plant as a whole was washed off in water to eliminate the dust, then rinsed in distilled water, and dried in the shade at room temperature. After that, a mortar and pestle were used to grind the dry plant into powder form. 10 g of the plant powder was mixed with 100 mL of distilled water in a conical flask, and the mixture was constantly stirred at room temperature on an orbital shaker for 72 h. The Whatman filter paper was used to filter the mixture. After that, the plant extract was kept in the refrigerator for further analysis.

2.2. Green Synthesis of Pure and Zr-Doped CeO_2 NPs. In this analysis, 30 mL of 0.5 M solution of Ce $(NO_3)_3.6H_2O$) was mixed into 10 mL of an aqueous plant extract of *Sanvitalia procumbens* that acts as a capping and reducing agent for the synthesis of pure CeO_2 NPs. Then, the reaction solution was agitated for 30 min at 1300 rpm to form a homogenous mixture. The solution mixture was calcined at 500°C for 2 h. A mortar and pestle were used to grind the obtained pure NPs into its powder form. Furthermore, the synthesis of Zr-doped CeO_2 NPs was achieved with the variation x ($x = 5\%$, 10%, and 15%) of ZrO $(NO_3)_2$. xH_2O (zirconium (IV) oxynitrate hydrate, without further purification) solution. In this analysis, Ce $(NO_3)_3{\cdot}6H_2O$) was mixed into the solution of ZrO $(NO_3)_2{\cdot}xH_2O$) with a ratio of 1:10, 1:5, and 1:3 v/v yielding final solution of 5%, 10%, and 15% Zr-doped CeO_2 NPs. After that, pH 8 was adjusted during the reaction and the mixture was heated at 80°C for 5-6 h to achieve the optimal reaction temperature. Finally, a muffle furnace was used for the calcination which took place at 450°C for 5 h. The 5%, 10%, and 15% Zr-doped CeO_2 NPs were obtained in a yellowish-white color, which were used for further characterization and biological screening [25].

2.3. Characterization of Pure and Zr-Doped CeO_2 NPs

2.3.1. PXRD Analysis. The X-ray diffractometer (PAN analytical X-Pert PRO) was run at 40 kV and 30 mA to analyze the X-ray diffraction (PXRD) of all samples. A Cu-Ka radiation at 1.54056 Å was used to obtain the pattern. The crystalline nature, crystallite size, and phase purity of the NPs were assessed in 20°–70° at 2θ range, at a scanning speed of 2°/min.

2.3.2. FT-IR Analysis. The synthesis of pure and Zr-doped CeO_2 NPs was achieved in the presence of phytoconstituents that serve as reducing, stabilizing, and capping agents. The phytoconstituents obtained in FT-IR analysis were examined using a KBr pellet system (Bruker, Alpha-II, Billerica, MA, USA). The samples were analyzed using FT-IR with resolutions of 4 cm^{-1} and wavenumber ranges between 4000 and 500 cm^{-1}.

2.3.3. SEM Analysis. A SEM image (SEM-JEOL JSM 6390) was used to determine the surface structure of pure and Zr-doped CeO_2 NPs. The instrument was operated at 15 kV accelerating voltage to capture the SEM images.

2.3.4. EDX Analysis. The NPs were dried on a carbon-coated copper grid for this investigation and were examined using EDX before being put through a SEM with a thermos EDX attachment.

2.3.5. UV-Vis Spectroscopy. The UV-Vis spectrophotometer (Shimadzu-UV-1800) was commonly employed to examine the reduction of cerium salt into CeO_2 NPs. The sample of pure and Zr-doped CeO_2 NPs was analyzed with a UV-Vis spectrophotometer, after being diluted with distilled water. The distilled water was used to fill the quartz cuvette cell which served as a standard for measuring the spectrum wavelength at 200–700 nm scanning rate.

2.4. Cytotoxic Activity of Pure and Zr-Doped CeO_2 NPs. The IMR32 cell line (ATCC Number: CCL-127) was used to test the cytotoxicity of synthesized NPs using the MTT assay by SCINOSOL Pvt Ltd [26]. The cytotoxic activity of the synthesized NPs was revealed at different concentrations of 50, 100, 150, and 200 µg/mL. The drug doxorubicin (5 µL) was used as a positive control, while cell culture media were used as a negative control. The 96-well plate was first filled with a cell suspension containing 10^4 cells per well and then incubated for 24 h. The culture liquid was emptied from each well of the 96-well plate once it had been confirmed that the cells were sticking to the bottom of the plate. NPs were injected into the appropriate wells at a volume of 100 µL. After that, the plate was incubated at 37°C for 24 h with 5% CO_2. 10 μL of the MTT solution was added to each well of the 96-well plate, after removing the plate from the incubator. So, the plate was then reincubated for another 4 h. The percentage of cell viability (survival) was then determined after recoding the adsorption of each sample that was measured using an ELISA reader at a wavelength of 490 nm using the following equation:

$$\text{Cell Viability}\,(\%) = \left[100 \times \frac{(\text{sample abs})}{(\text{control abs})}\right], \qquad (1)$$

where the absorption of the test group is represented by (sample abs), the absorption of the control group is denoted by (control abs), and the cell viability is represented by (%).

2.5. Antiplatelet Activity. In order to prepare platelet-rich plasma (PRP) and platelet-poor plasma (PPP) from human blood cells, fresh humanoid plasma was collected for the experiment. The concentrations of platelets in PRP was adjusted with PPP to 3.1×10^8 platelets/m and sustained at 37°C for 2 h due to the aggregation process. Different

concentrations (10, 30, 50, 70, and 100 μg/mL) for pure, 5%, 10%, and 15% Zr-doped CeO_2 NPs were preincubated with human plasma (0.2 mL of citrated) in the presence of 10 mM Tris HCl (20 μL) buffer pH (7.4/L minutes at 37°C) to find out the plasma recalcification time (PRT). Once the mixture had been previously incubated, 20 μL of 0.25 M $CaCl_2$ was added, and the precipitation time was noted. A chronological dual channel was used to examine the platelet aggregation of green synthesized pure and various percentages of Zr-doped CeO_2 NPs. The reaction mixtures of pure and Zr-doped CeO_2 NPs were preincubated with PRP aliquots at various concentrations (10, 30, 50, 70, and 100 μg/mL), respectively. Thereafter, the addition of ADP (agonist) was to initiate the platelet aggregation independently and then followed for 6 min. The study revealed that both pure and Zr-doped CeO_2 NPs exhibited the platelet aggregation at different concentrations [27].

2.6. Statistical Analysis. The mean standard deviation ($n = 3$) was used to calculate the experimental results. One-way ANOVA GraphPad Prism version (10.0.1) was used to calculate the statistical analysis. ANOVA Analysis of variance using Tukey's HSD with significance of $p < 0.05$.

3. Results and Discussion

The green synthesis is an environmentally friendly and cost-effective method as compared to chemical method that diminishes the utilization of detrimental solvents and chemicals that are health hazards and non-ecofriendly. Additionally, green synthesis facilitates the use of free renewable resources found in nature. Plants are frequently used in green synthesis due to the availability of phytochemicals that function as reducing and stabilizing agents. Therefore, the current study was used to conduct the synthesis of NPs by using an aqueous extract of plant *Sanvitalia procumbens* [14]. Hence, the green fabricated pure and Zr-doped CeO_2 NPs via various percentages of dopant Zr (5%, 10%, and 15%) using plant extracts of *Sanvitalia procumbens* are given below.

3.1. PXRD Pattern of Pure and Zr-Doped CeO_2 NPs. The crystallinity of synthesized pure and Zr-doped CeO_2 NPs was examined using PXRD analysis. Figure 1 shows the peak diffraction of the PXRD patterns ranging from 20° to 70° at 2θ degrees for pure and Zr-doped CeO_2 NPs. The synthesized NPs indicate the structure of face-centered cubic by peaks obtained at 2θ of 28.21° (111), 33.01° (200), 47.30° (220), 56.57° (311), 59.36° (222), and 69.06° (400), which were corroborated from the standard card No. (JCPDS 00-004-0593). The obtained PXRD pattern for pure and Zr-doped CeO_2 NPs showed no additional peaks, showing that Zr^{4+} ions can successfully substitute Ce^{4+} in the CeO_2 lattice because of the small change in their ionic radii (Ce^{4+} 0.97 Å and Zr^{4+} 0.84 Å) [28]. Debye–Scherrer equation (2) was used to determine the mean particle size in order to enhance the effects of Zr dopant.

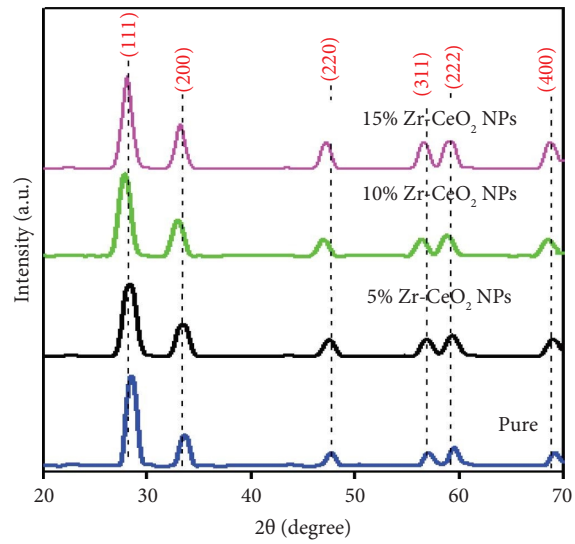


Figure 1: PXRD patterns of synthesized pure and Zr-doped CeO_2 NPs.

$$D = \frac{K\lambda}{\beta \cos\theta}, \tag{2}$$

where the particle size is represented by D, the symbol K denotes a crystalline nature of dimensionless factor that was usually 0.9, λ is used to denote the X-ray wavelength, the FWHM (full width at half maximum) of the samples was expressed by β, and the angle of diffraction is represented by symbol θ. The mean particle size of each sample has been calculated using Scherrer's equation from the FWHM of the peaks, which were indexed (111) at 28.21°. The mean particle diameters were determined to be 5.77, 6.54, 7.18, and 5.14 nm for pure, 5%, 10%, and 15% Zr-doped CeO_2 NPs, respectively. The result demonstrates that 15% Zr-doped CeO_2 NPs revealed the smaller mean crystallite size in comparison to pure and other doping NPs. Hence, there was a small increase in the size of the NPs as well as the strength of the diffraction peaks with increasing Zr dopant concentrations (from pure to 10% Zr-doped CeO_2 NPs). If further increase the doping percentage of Zr, the average size of Zr-doped CeO_2 NPs was the decreases (15% Zr-doped CeO_2 NPs). The results revealed that the diffraction peak intensity was slightly increased as compared to pure NPs with increasing percentage of Zr dopant. Thus, the crystalline nature of CeO_2 NPs was improved with doping. The average crystallite size was found to be changed as a result of the Zr^{4+} ion substitution with respect to Ce^{4+} ion in the CeO_2 NPs. The stoichiometry of the NPs may have been altered by the Zr doping which introduces the crystal defects that led to balance in charge. The concentration and mobility of oxygen vacancies are enhanced to ensure charge neutrality, which modifies the characteristics of the NPs [29]. A comparable investigation by Laguna et al. demonstrated that the Zr dopant reduced average size of crystalline NPs [30]. Likewise, Kumar and Jaya reported that the addition of a tin dopant reduced the crystallite size of synthesized ceria [31].

3.2. FT-IR Analysis of Pure and Zr-Doped CeO_2 NPs. The functional groups of organic molecules or phytochemicals present in an aqueous plant extract that serve as oxidizing and capping agents for the synthesis of NPs were identified using FT-IR analysis. Figure 2 of the FT-IR analysis of the *Sanvitalia procumbens* plant extract shows different bands that are similar to those in our previously published articles [32, 33]. The FT-IR spectrum of pure, 5%, 10%, and 15% Zr-doped CeO_2 NPs revealed absorption band ranges between 400 and 4000 cm^{-1} wavenumber as mentioned in Figure 2. The strong vibrational peaks were detected in all samples at a range of 3300 to 3200 cm^{-1}, which resembles the -OH group of stretching vibrational modes of the phenols and alcohols. The broad peaks around 3300–3200 cm^{-1} in the FT-IR spectrum may be caused by the intermolecular hydrogen bonds of the polyphenolic functional group [34]. The FT-IR bands observed stretching vibration at 1600–1500 cm^{-1} that were caused by the C = O functional group of amides. However, it was observed that as the Zr doping was increased, the peaks became more overlapping and revealed less intensity absorption band. The IR band of all spectra ranges at 1300 cm^{-1} was represented by stretching rock mode for C-H group of organic molecules [35]. The C-O band of the functional group of alcohol was responsible for the peaks observed at 1100–1050 cm^{-1}. The band of absorption at 840 cm^{-1} corresponds to the stretching vibration of Ce-O and also for doped NPs that was used to validate the synthesis of pure and Zr-doped CeO_2 NPs in all synthesized samples [36]. The obtained results for pure and Zr-doped CeO_2 NPs showed a shift in the peaks indicating the existence of functional groups in the plant extract that could be due to alkaloids, proteins, flavonoids, phenols, and steroids present in the extract and are responsible for NP synthesis. Similarly, the intensity of the absorption band decreases and shifts toward the lower wavenumber by increasing the percentage of Zr dopant [37]. There is no specific literature available on synthesis of plant-mediated doped and undoped CeO_2 NPs. However, the polyphenolic chains present in *Sanvitalia procumbens* play a significant role in the synthesis of the NPs. The phytoconstituents of plant extract also correspond to the aromatic carbons along with metabolites like proteins, flavonoids, and alkaloids that surround the Ce^{3+} and Zr^{4+} metal ions leading to the formation of pure and Zr-doped CeO_2 NPs. Thus, the study showed that plant extract contains essential phytoconstituents that may have ability to synthesize the stable synthesis of doped and undoped metal oxide [36].

3.3. SEM Analysis of Pure and Zr-Doped CeO_2 NPs. SEM images were used to examine the morphology of pure and Zr-doped CeO2 NPs, as shown in Figure 3. The doping of Zr ion into crystal lattice of CeO_2 NPs showed an impact on size and morphology of synthesized NPs. The given SEM micrograph revealed an irregular morphology of pure, 5%, 10%, and 15% Zr-doped CeO_2 NPs. It has been demonstrated that the phytochemicals that exist in plant extract of *Sanvitalia procumbens* act as a stabilizing agent which can kinetically influence the formation rate of surface metal oxide NPs [38].

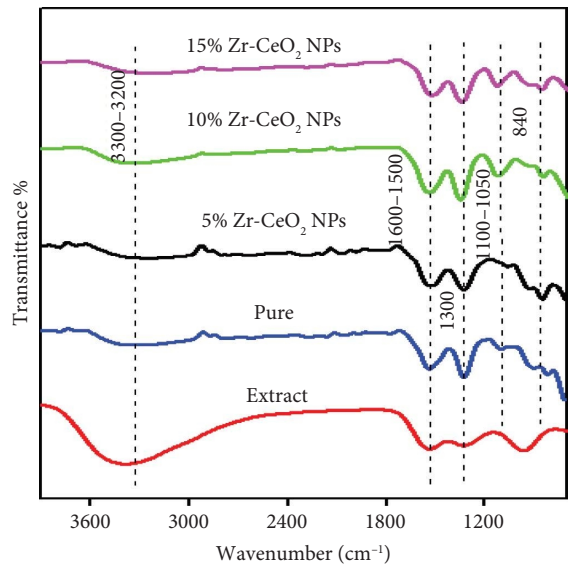


Figure 2: FT-IR spectrum of synthesized pure, Zr-doped CeO_2 NPs, and aqueous plant extract.

Figure 3(A) shows the agglomerated irregular spheres in pure NPs with size range of 26.72 nm, whereas the average particle sizes of 5% Zr-doped CeO_2 NPs showed 24.37 nm that exhibit blurry impression, which could be interpreted by the plant compounds coated on exterior surfaces. The 10% and 15% Zr-doped CeO_2 NPs revealed 21.24 and 19.12 nm particle size with agglomerated and surface smooth morphology (Figures 3(C) and 3(D)). The aggregation was observed in SEM images, which could be due to the effect of steric as well as attractive van der Waals forces that exist in synthesized NPs. Hence, the small size NPs have a higher surface area-to-volume ratio and stronger attractive forces and causes to increasing an agglomeration. It has been noted that the average particle size was changed by the addition of Zr ion into CeO_2 NPs. Thus, the results revealed that 5%, 10%, and 15% Zr-doped CeO_2 NPs showed similar morphology to that of pure CeO_2 NPs, but the size of NPs varies from one another. This was because different crystallographic facets may interact unevenly with a capping reagent or polymeric material, resulting in an uneven rate of formation in all directions [39]. Similar results were obtained using previously reported literature [28].

3.4. EDX Analysis of Pure and Zr-Doped CeO_2 NPs. The EDX spectroscopic techniques were used to ascertain the fundamental chemistry of the synthesized NPs, as illustrated in Figure 4. The study revealed that pure CeO_2 NPs and 5% Zr-doped CeO_2 NPs contain strong signal of cerium (Ce) and oxygen (O) indicating the essential elements that are present in the structural composition of NPs. However, the spectroscopic analysis of 10%, and 15% Zr-doped CeO_2 NPs exhibits the peak of Ce and O and Zr element which confirmed the successful incorporation of Zr ions into the CeO_2 crystal structure by doping. The weight percentage of Ce and O in pure NPs was 42.95% and 23.78%, respectively, whereas the weight percentages of Ce and O were increased in 5% Zr-

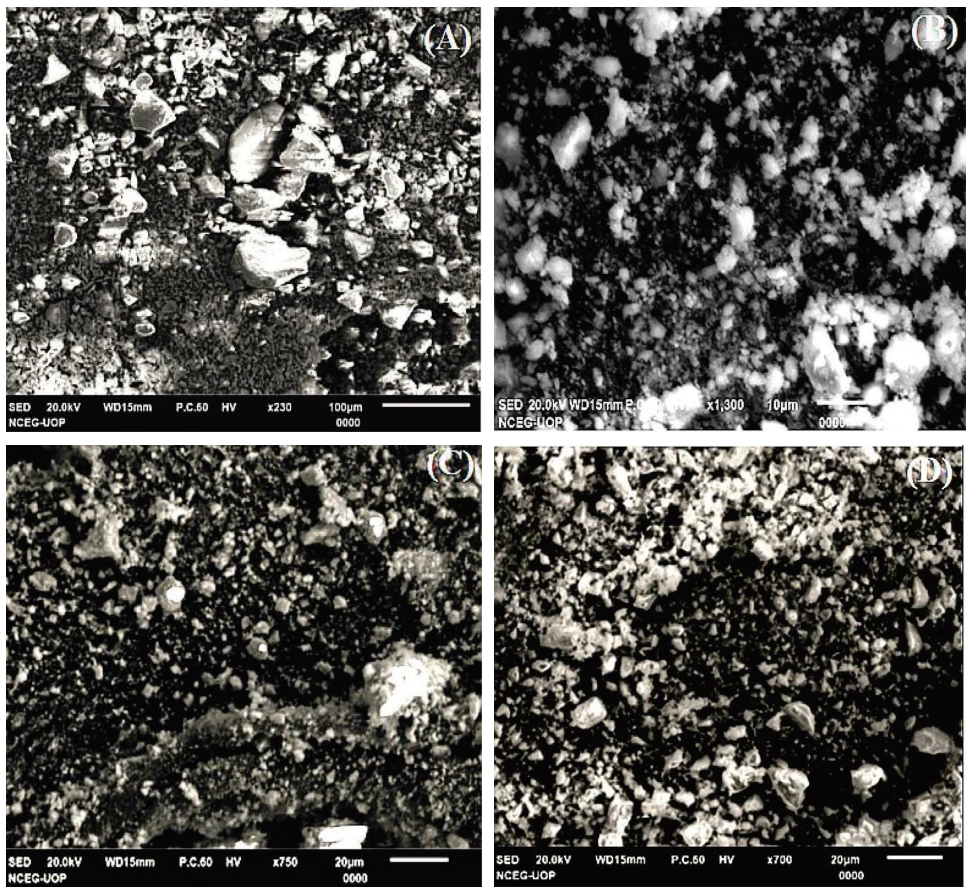


Figure 3: SEM images of (A) pure, (B) 5% Zr-doped CeO_2 NPs, (C) 10% Zr-doped CeO_2 NPs, and (D) 15% Zr-doped CeO_2 NPs.

doped CeO_2 NPs that were 71.63% and 17.60%, respectively. The 10% Zr-doped CeO_2 NPs showed 25.24%, 32.68%, and 13.72% for Ce, O, and Zr. Similarly, the weight percentage for Ce, O, and Zr in 15% Zr-doped CeO_2 NPs was 12.25%, 34.19%, and 26.40%, respectively. The finding showed that pure CeO_2 NPs exhibit a strong signal for Ce, indicating the successful synthesis of NPs. However, the 5% Zr-doped CeO_2 NPs exhibit strong Ce and O peak and did not show any Zr peak indicating that the small percentage of Zr-doped CeO_2 NPs or an uneven distribution of doped elements in the sample may cause the electron beam to fail to interact with the doped regions, resulting in the absence of Zr signals, whereas the 10% and 15% Zr-doped CeO_2 NPs showed strong Zr signals indicating the doping of Zr into CeO_2 NPs that reduces the signal of Ce and O in the EDX analysis. The result indicates that weight percentage of Zr ions into the CeO_2 NPs increases by increasing the percentage of Zr doping [28].

3.5. UV-Vis Analysis of Pure and Zr-Doped CeO_2 NPs. UV-Vis spectroscopy was used to analyze the optical spectra of pure and Zr-doped CeO_2 NPs. The absorption spectra of UV-Vis for Zr-doped CeO_2 NPs at different percentages (5%, 10%, and 15%) are illustrated in Figure 5. The *Sanvitalia procumbens* plant extract did not show any obvious peak in the visible region of UV-Vis spectrophotometer that is similar to those of our previously published report [32]. However, a mixture of $Ce(NO_3)_3{\cdot}6H_2O$) and plant extract was used to validate the synthesis of CeO_2 NPs. The surface plasmon resonance (SPR) peak becomes readily visible in an aqueous colloidal solution due to the significant absorption of optical spectra, which are mostly acquired at 305 nm for pure NPs. Meanwhile, the absorption spectra of the remaining Zr dopant exhibit at around 295, 286, and 272 nm for 5%, 10%, and 15% of Zr-doped CeO_2 NPs, respectively. The absorbance peaks of Zr-doped CeO_2 NPs were somewhat shifted toward the lower wavelength due to the incorporation of Zr doping. The incorporation of the smaller Zr^{4+} ions (ionic radius of 0.84 Å) into the lattice structure of CeO_2 (ionic radius of Ce^{4+} is 0.97 Å) results in formation of oxygen vacancies and lattice distortion that leads to change the electronic structure of CeO_2 NPs. This causes the blue shift (lower wavelength) in UV-Vis absorption peak of Zr-doped CeO_2 NPs. The blue shift observed in UV-Vis analysis by Zr doping modifies the electronic structure and widens the band gap energy of CeO_2 NPs. The band gap energy Eg(D) for optical spectra can be measured by using the following equation:

$$\alpha h\nu = ED\,(h\nu - Eg)^{1/2}, \tag{3}$$

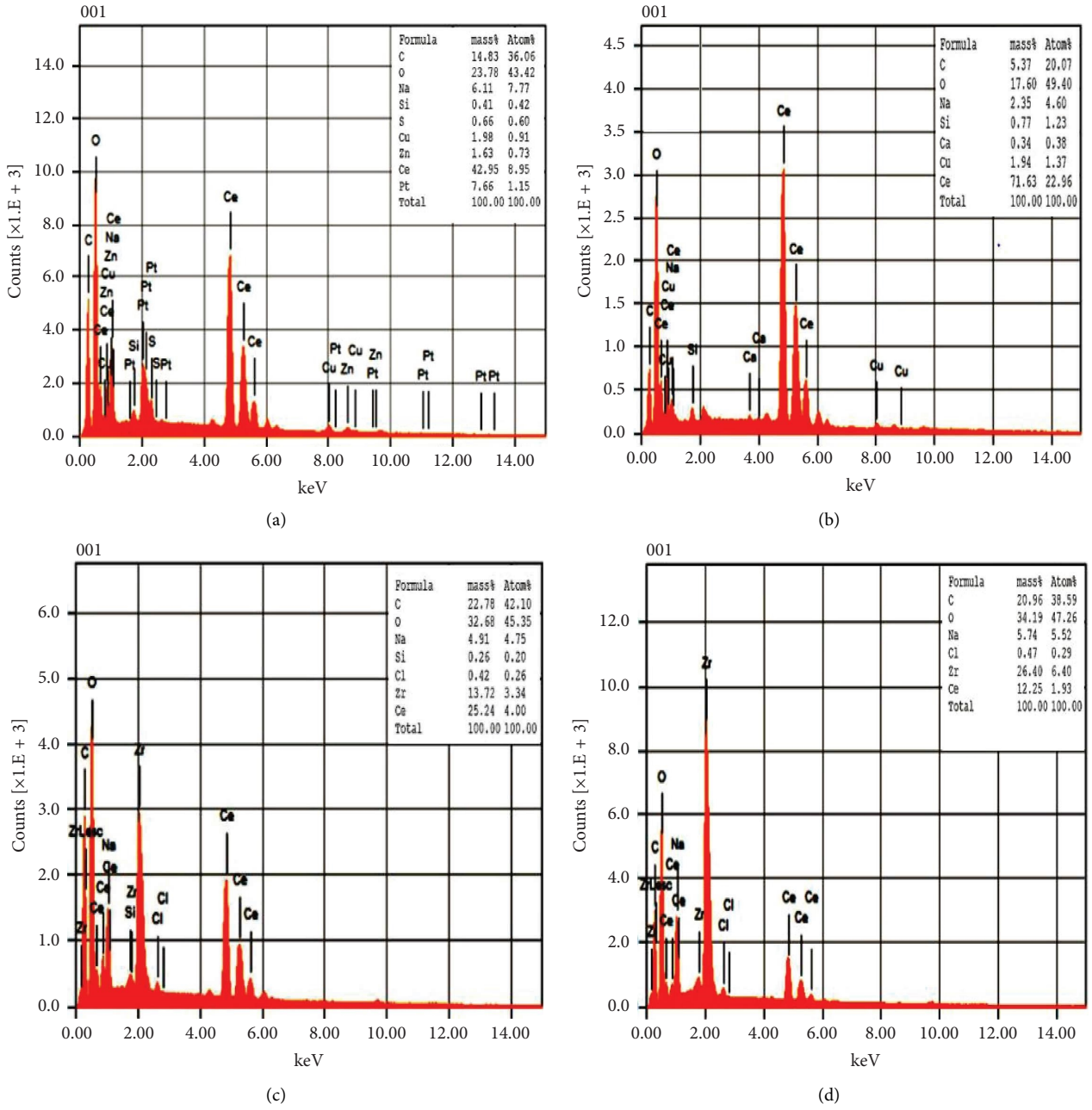


Figure 4: EDX analysis for (a) pure, (b) 5% Zr-doped CeO_2 NPs, (c) 10% Zr-doped CeO_2 NPs, and (d) 15% Zr-doped CeO_2 NPs.

where $h\nu$ is used to denote the photon energy, α symbol represents the optical absorption coefficient, ED is used as a constant, and Eg corresponds to the direct band gap energy. The band gap energy obtained for pure, 5%, 10%, and 15% Zr-doped CeO_2 NPs was corresponding to 4.07, 4.20, 4.43, and 4.56 eV, respectively. It was found that increasing the percentage of dopant led to a slight increase in the band gap energy of the Zr-doped CeO_2 NPs. This indicates that the percentage of dopant depends on band gap energy. However, the narrow band gap energy difference of each of these NPs suggests that the NPs are capable of being visible light active [40]. Furthermore, the particle size of semiconductor NPs is inversely correlated with the band gap energy that decreases by increasing the percentage of Zr doping [41]. This relationship is due to the quantum confinement theory that supported the obtained size-dependent band gap energy Eg(D) of synthesized NPs. The evidence suggests that the potential barriers on the surface of the quantum box confine the electrons in the conduction band and the holes in the valence band. The electron and hole confinement causes the increase in band gap energy between the valence band and the conduction band with decreasing particle size [38]. Thus, the anticipated outcomes correspond with those of previously published literature [5].

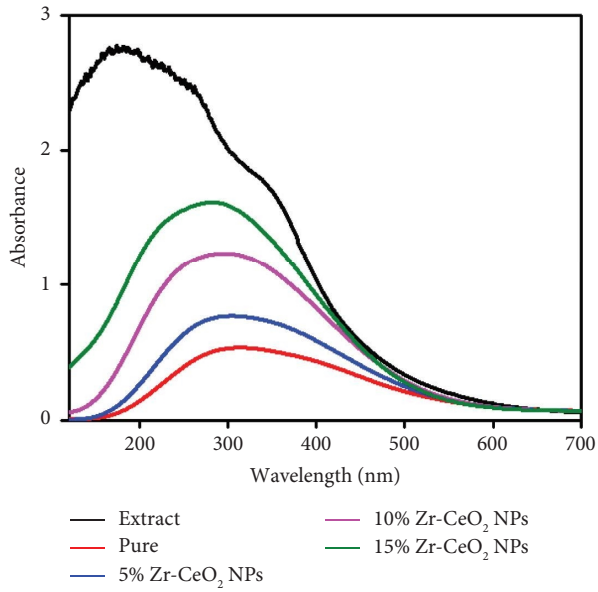


Figure 5: UV-visible spectra of synthesized pure and Zr-doped CeO_2 NPs.

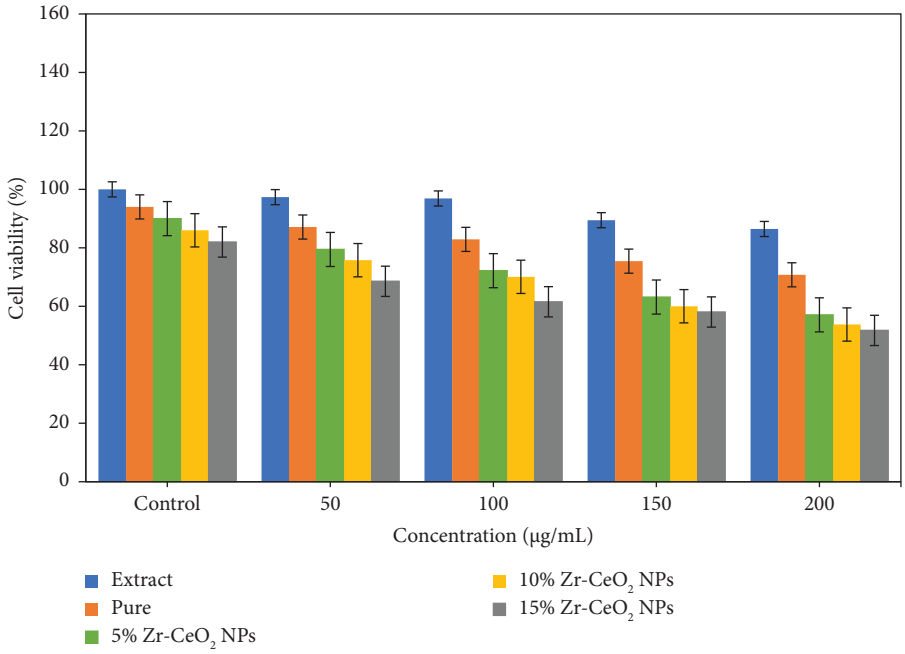


Figure 6: % cell viability of pure and Zr-doped CeO_2 NPs at different concentrations (μg/mL).

3.6. Biocompatibility Assessment

3.6.1. Cytotoxicity Results. The cytotoxic activity of the synthesized NPs was assessed by using MTT assay on the IMR32 cancer cell line. Figure 6 shows the cell viability of extract, pure, 5%, 10%, and 15% Zr-doped CeO_2 NPs, which revealed that the cell viability of synthesized NPs decreases with increasing concentrations of NPs. Thus, the concentration-dependent cytotoxic activity was obtained on IMR32 cell line. The cytotoxic effects of 5%, 10%, and 15% Zr-doped CeO_2 NPs were analyzed to demonstrate the impact of cytotoxicity on cancerous cells which was more significantly decreased in contrast to extract and undoped CeO_2 NPs. It was observed that 15% Zr-doped CeO_2 NPs induce 51.76% of cancer cell viability at 200 μg/mL concentrations. The findings show that 15% Zr-doped CeO_2 NPs showed remarkable cytotoxic activity against cancer cells. Thus, the findings demonstrate that significant cytotoxic activity was observed at 200 μg/mL of Zr-doped CeO_2 NPs, which displays greater inhibition of the proliferation of cancer cells. This suggests that synthesized NPs may have ability to induce the generation of ROS which improve the

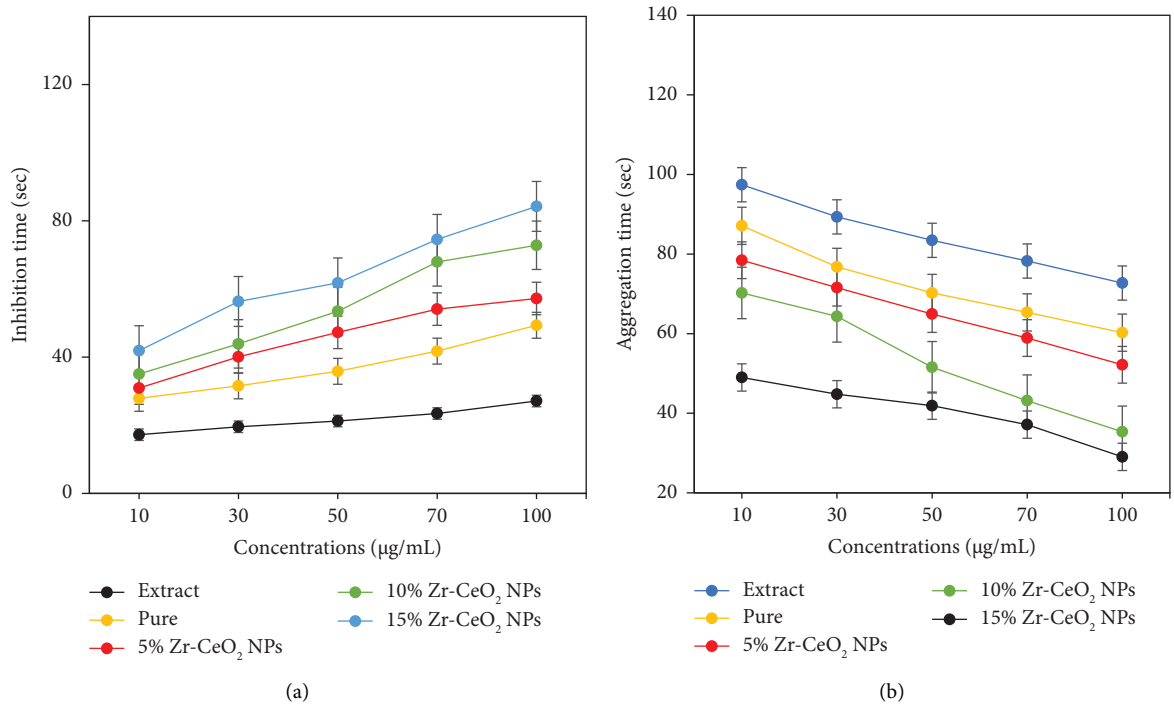


Figure 7: Antiplatelet activity of green synthesized pure, 5%, 10%, and 15% Zr-doped CeO_2 NPs using ADP as agonists. (a) Effect of dose-dependent platelet inhibition time (sec). (b) Effect of dose-dependent platelet aggregation time (sec).

inhibition of tumor cells by damaging cellular components. Moreover, the shape and size of Zr-doped CeO_2 NPs also showed significant function in cytotoxic activity that triggers the apoptosis in the cell lines [26]. The size obtained in 15% Zr-doped CeO_2 NPs was very small which can easily enter into the cancer cells. It disrupts the function of mitochondria and DNA which leads to the death of cancer cells [42]. Moreover, the NPs also make it possible for ROS production and can induce oxidative stress that have a significant impact on the inhibition of tumor cell growth [43]. Similarly report available on the cytotoxic activity of Zr-doped CeO_2 NPs that showed more potent cytotoxic effects on various cancer cell lines, such as HeLa, MCF-7, and A549 cells [44]. Another study reports that 10% Zr-doped CeO_2 NPs demonstrated higher cytotoxicity against HepG2 liver cancer cells. This is because the Zr-doped CeO_2 NPs may have the ability to enhance the generation ROS that causes the apoptosis and cell cycle arrest in the cancer cells [28].

3.7. Biological Screening

3.7.1. Antiplatelet Activity. Platelets are important components in the bloodstream that play a key function in blood clotting during a wound or an injury in accident. In the physiological impact, ADP acts as an agonist by binding site to receptors on the platelet membrane, which requires necessary modifications to confirm the aggregation in the platelets. The presence of clotting characteristics in the area of wounds was responsible for activated platelets that showed a crucial function in the mesh development, which prevents blood loss at the time of injury and other disorders. However, hyper-initiation of platelets which have the characteristic symptoms of thrombotic disorder caused severe diseases. Therefore, an antagonist that stops agonists from binding to the receptors on the surface of platelets may be an advanced antiplatelet medication that prevents platelet hyperactivation. The study investigated the antiplatelet activity of green synthesized NPs, including pure, 5%, 10%, and 15% Zr-doped CeO_2 NPs, against common ADP, demonstrating both agonist and antagonistic properties. Figure 7 illustrates how the ADP-induced platelet aggregation was prevented by the green synthesized doped and undoped CeO_2 NPs. The impact of pure, 5%, 10%, and 15% Zr-doped CeO_2 NPs on the prevention of ADP-induced aggregation of platelets is depicted in Figure 7(a). The synthesized NPs inhibit the maximum platelet aggregation to an extent of 27.12, 49.35, 57.21, 72.83, and 84.24 s for extract, pure, 5%, 10%, and 15% Zr-doped CeO_2 NPs at concentrations of 100 μg/mL, respectively. According to Figure 7(b), the effect of NPs (100 μg/mL) on platelet aggregation was 29.04, 53.18, 62.25, 72.72, and 84.24 s for extract, pure, 5%, 10%, and 15% Zr-doped CeO_2 NPs, respectively. The finding demonstrates that antiplatelet activity of all samples extracts, pure, 5%, 10%, and 15% Zr-doped CeO_2 NPs, showed significant results at 100 μg/mL concentrations, whereas the synthesized samples showed slightly different results at concentrations lower than 100 μg/mL. The obtained result suggests that antiplatelet activity was enhanced with increasing concentrations of Zr doping into CeO_2 NPs. The 5% and 10% Zr-doped CeO_2 NPs exhibit moderate activity as compared to 15% Zr-doped CeO_2 NPs that showed significant antiplatelet activity. Hence, the results conclude that doped NPs can be more active

antiplatelet agents than undoped NPs to cure health-related diseases [45]. The Zr-doped CeO_2 NPs play an important role in antiplatelet therapy involving the binding of specific agonists, such as ADP to the platelet surface, and appear as a treatment for thrombosis under physiological conditions. The platelet aggregation is ultimately caused by the activation of the IIb/IIIa (GP IIb/IIIa) pathway of glycoprotein, which is activated by the binding of ADP to the platelet. The GP IIb/IIIa receptor binds to fibrinogen and aids in the formation of platelet crosslinks that lead to platelet aggregation. Thus, platelet aggregation and platelet plug formation take place. The uncontrolled platelet activation and aggregation are key factors in thrombotic diseases [46]. The study concludes that NPs can activate platelets through the GP IIb/IIIa pathway, triggering the ADP-mediated receptor activation and fibrinogen binding, thereby promoting platelet crosslinking and thrombus formation. The result of the antiplatelet activity was consistent to those of the previously reported literature [47].

4. Conclusion

The current study was based on an environmentally friendly method used for the synthesis of pure, 5%, 10%, and 15% Zr-doped CeO_2 NPs using plant extract of *Sanvitalia procumbens*. The synthesized NPs were characterized by different analytical techniques including UV-Vis, SEM, PXRD, FT-IR, and EDX analysis. Furthermore, the synthesized NPs exhibit potential antiplatelet activity which was enhanced using Zr-doped CeO_2 NPs. The results show that Zr-doped CeO_2 NPs effectively inhibit platelet aggregations and can be more active against health disorders. The cytotoxicity of synthesized NPs revealed that 15% Zr-doped CeO_2 NPs were biologically compatible at concentrations of 200 μg/mL. Thus, the future studies should be continued on synthesizing CeO_2 NPs with different metal doping that has a higher potential of platelet aggregation and inhibiting cancer cell proliferation, suggesting potential applications in the biomedical field.

Data Availability Statement

The data that support the findings of this study are available from the corresponding authors upon reasonable request.

Ethics Statement

The ethical approval of the project was issued by the KUST Ethical Committee under reference No. Ref, No, /KUST/ Ethical Committee/386 dated 01 July 2022.

Conflicts of Interest

The authors declare no conflicts of interest.

Author Contributions

Conceptualization, I.A. and F.F.; data curation, I.A.; formal analysis, T.P., I.A., S.S.A.-R., Z.Z., M.M.L., and F.F.; funding acquisition, M.M. and F.F.; investigation, T.P.; methodology, T.P.; project administration, I.A.; resources, I.A.; supervision: I.A. and F.F.; visualization, M.A. and M.M.; writing–original draft, T.P., M.A., and A.K.; and writing–review and editing, I.A., F.F., M.M., S.S.A.-R., Z.Z., and M.M.L. The authors have accepted responsibility for the entire content of this manuscript and approved its submission.

Funding

This work was funded by the Researchers Supporting Project (RSPD2025R758), King Saud University, Riyadh, Saudi Arabia. The publication charges for this article are partially borne from Khyber Medical University Publication Fund (No. DIR/ORIC/Ref/24/00046).

Acknowledgments

The authors extend their appreciation to the Researchers Supporting Project (RSPD2025R758), King Saud University, Riyadh, Saudi Arabia.

References

[1] P. Eriksson, A. A. Tal, A. Skallberg, et al., "Cerium Oxide Nanoparticles With Antioxidant Capabilities and Gadolinium Integration for MRI Contrast Enhancement," *Scientific Reports* 8, no. 1 (2018): 6999, https://doi.org/10.1038/s41598-018-25390-z.

[2] S. K. Kannan and M. Sundrarajan, "A Green Approach for the Synthesis of a Cerium Oxide Nanoparticle: Characterization and Antibacterial Activity," *International Journal of Nanoscience* 13, no. 03 (2014): 1450018, https://doi.org/10.1142/s0219581x14500185.

[3] D. G. Shchukin and R. A. Caruso, "Inorganic Macroporous Films From Preformed Nanoparticles and Membrane Templates: Synthesis and Investigation of Photocatalytic and Photoelectrochemical Properties," *Advanced Functional Materials* 13, no. 10 (2003): 789–794, https://doi.org/10.1002/adfm.200304415.

[4] A. C. Sajeevan and V. Sajith, "A Study on Oxygen Storage Capacity of Zirconium-Cerium-Oxide Nanoparticles," *Advanced Materials Research* 685 (2013): 123–127, https://doi.org/10.4028/www.scientific.net/amr.685.123.

[5] R. Bakkiyaraj, M. Balakrishnan, G. Bharath, and N. Ponpandian, "Facile Synthesis, Structural Characterization, Photocatalytic and Antimicrobial Activities of Zr Doped CeO2 Nanoparticles," *Journal of Alloys and Compounds* 724 (2017): 555–564, https://doi.org/10.1016/j.jallcom.2017.07.049.

[6] P. Sagar Vijay Kumar, L. Suresh, T. Vinodkumar, B. M. Reddy, and G. V. P. Chandramouli, "Zirconium Doped Ceria Nanoparticles: An Efficient and Reusable Catalyst for a Green Multicomponent Synthesis of Novel Phenyldiazenyl–Chromene Derivatives Using Aqueous Medium," *ACS Sustainable Chemistry & Engineering* 4, no. 4 (2016): 2376–2386, https://doi.org/10.1021/acssuschemeng.6b00056.

[7] M. R. Dumont, E. H. Nunes, and W. L. Vasconcelos, "Use of a Design-of-Experiments Approach for Preparing Ceria–Zirconia–Alumina Samples by Sol–Gel Process," *Ceramics International* 42, no. 8 (2016): 9488–9495, https://doi.org/10.1016/j.ceramint.2016.03.021.

[8] G. Feng, W. Han, Z. Wang, F. Li, and W. Xue, "Highly Reducible Nanostructured CeO2 for CO Oxidation,"

Catalysts 8, no. 11 (2018): 535, https://doi.org/10.3390/catal8110535.

[9] J. Deng, S. Li, L. Xiong, et al., "Preparation of Nanostructured CeO2-ZrO2-Based Materials With Stabilized Surface Area and Their Catalysis in Soot Oxidation," *Applied Surface Science* 505 (2020): 144301, https://doi.org/10.1016/j.apsusc.2019.144301.

[10] Y. Huang, C. An, Q. Zhang, et al., "Cost-Effective Mechanochemical Synthesis of Highly Dispersed Supported Transition Metal Catalysts for Hydrogen Storage," *Nano Energy* 80 (2021): 105535, https://doi.org/10.1016/j.nanoen.2020.105535.

[11] K. K. Brar, S. Magdouli, A. Othmani, et al., "Green Route for Recycling of Low-Cost Waste Resources for the Biosynthesis of Nanoparticles (NPs) and Nanomaterials (NMs)-A Review," *Environmental Research* 207 (2022): 112202, https://doi.org/10.1016/j.envres.2021.112202.

[12] S. Matussin, M. H. Harunsani, A. L. Tan, and M. M. Khan, "Plant-Extract-Mediated SnO2 Nanoparticles: Synthesis and Applications," *ACS Sustainable Chemistry & Engineering* 8, no. 8 (2020): 3040–3054, https://doi.org/10.1021/acssuschemeng.9b06398.

[13] Q. Maqbool, M. Nazar, S. Naz, et al., "Antimicrobial Potential of Green Synthesized CeO2 Nanoparticles From Olea Europaea Leaf Extract," *International Journal of Nanomedicine* 11 (2016): 5015–5025, https://doi.org/10.2147/ijn.s113508.

[14] R. Magudieshwaran, J. Ishii, K. C. N. Raja, et al., "Green and Chemical Synthesized CeO2 Nanoparticles for Photocatalytic Indoor Air Pollutant Degradation," *Materials Letters* 239 (2019): 40–44, https://doi.org/10.1016/j.matlet.2018.11.172.

[15] J. T. Dahle and Y. Arai, "Environmental Geochemistry of Cerium: Applications and Toxicology of Cerium Oxide Nanoparticles," *International Journal of Environmental Research and Public Health* 12, no. 2 (2015): 1253–1278, https://doi.org/10.3390/ijerph120201253.

[16] F. Javadi, M. E. Taghavizadeh Yazdi, M. Baghani, and A. Es-haghi, "Biosynthesis, Characterization of Cerium Oxide Nanoparticles Using Ceratonia Siliqua and Evaluation of Antioxidant and Cytotoxicity Activities," *Materials Research Express* 6, no. 6 (2019): 065408, https://doi.org/10.1088/2053-1591/ab08ff.

[17] M. Soh, D. W. Kang, H. G. Jeong, et al., "Ceria–Zirconia Nanoparticles as an Enhanced Multi-antioxidant for Sepsis Treatment," *Angewandte Chemie* 129, no. 38 (2017): 11557–11561, https://doi.org/10.1002/ange.201704904.

[18] A. Lateef, M. A. Akande, S. A. Ojo, B. I. Folarin, E. B. Gueguim-Kana, and L. S. Beukes, "Paper Wasp Nest-Mediated Biosynthesis of Silver Nanoparticles for Antimicrobial, Catalytic, Anticoagulant, and Thrombolytic Applications," *Biotech* 6, no. 2 (2016): 140–210, https://doi.org/10.1007/s13205-016-0459-x.

[19] S. Peeters Weem, S. T. W. Van Haelst, H. M. Den Ruijter, F. L. Moll, and G. J. De Borst, "Lack of Evidence for Dual Antiplatelet Therapy After Endovascular Arterial Procedures: A Meta-Analysis," *European Journal of Vascular and Endovascular Surgery* 52, no. 2 (2016): 253–262, https://doi.org/10.1016/j.ejvs.2016.04.023.

[20] R. N. Krishnaraj and S. Berchmans, "In Vitro Antiplatelet Activity of Silver Nanoparticles Synthesized Using the Microorganism Gluconobacter Roseus: An AFM-Based Study," *RSC Advances* 3, no. 23 (2013): 8953–8959, https://doi.org/10.1039/c3ra41246f.

[21] J. W. Eikelboom, J. Hirsh, J. I. Weitz, M. Johnston, Q. Yi, and S. Yusuf, "Aspirin-Resistant Thromboxane Biosynthesis and the Risk of Myocardial Infarction, Stroke, or Cardiovascular Death in Patients at High Risk for Cardiovascular Events," *Circulation* 105, no. 14 (2002): 1650–1655, https://doi.org/10.1161/01.cir.0000013777.21160.07.

[22] A. M. Torres, *Revision of Sanvitalia (Compositae-Heliantheae)* (Brittonia, 1964).

[23] M. L. Pérez-Ochoa, J. L. Chávez-Servia, A. M. Vera-Guzmán, E. N. Aquino-Bolaños, and J. C. Carrillo-Rodríguez, "Medicinal Plants Used by Indigenous Communities of Oaxaca, Mexico, to Treat Gastrointestinal Disorders," *Pharmacognosy Medicinal Plants* (2016).

[24] L. Wang, T. Wang, Q. S. Guo, Y. Huang, and H. K. Xu, "Comparative study on Four Major Active Compounds of *Sanvitalia procumbens* and Chrysanthemum Morifolium Cv Hangju and Gongju," *China Journal of Chinese Materia Medica* 38, no. 20 (2013): 3442–3445.

[25] U. K. Mishra, V. S. Chandel, O. P. Singh, and N. Alam, "Synthesis of CeO_2 and Zr-Doped CeO_2 (Ce1−x $ZrxO_2$) Catalyst by Green Synthesis For Soot Oxidation Activity," *Arabian Journal for Science and Engineering* 48 (2022): 771–777, https://doi.org/10.1007/s13369-022-06997-x.

[26] K. Hamidian, M. R. Saberian, A. Miri, F. Sharifi, and M. Sarani, "Doped and Un-Doped Cerium Oxide Nanoparticles: Biosynthesis, Characterization, and Cytotoxic Study," *Ceramics International* 47, no. 10 (2021): 13895–13902, https://doi.org/10.1016/j.ceramint.2021.01.256.

[27] K. Lingaraju, R. B. Basavaraj, K. Jayanna, et al., "Biocompatible Fabrication of TiO_2 Nanoparticles Antimicrobial, Anticoagulant, Antiplatelet, Direct Hemolytic and Cytotoxicity Properties," *Inorganic Chemistry Communications* 127 (2021): 108505, https://doi.org/10.1016/j.inoche.2021.108505.

[28] S. N. Naidi, F. Khan, M. H. Harunsani, A. L. Tan, Y. M. Kim, and M. M. Khan, "Effect of Zr Doping on Photoantioxidant and Antibiofilm Properties of CeO_2 NPs Fabricated Using Aqueous Leaf Extract of Pometia Pinnata," *Bioprocess and Biosystems Engineering* 45 (2022): 279–295, https://doi.org/10.1007/s00449-021-02656-x.

[29] A. T. Apostolov, I. N. Apostolova, and J. M. Wesselinowa, "A Comparative Study of the Magnetization in Transition Metal Ion Doped CeO_2, TiO_2 and SnO_2 Nanoparticles," *Physica E: Low-Dimensional Systems and Nanostructures* 99 (2018): 202–207, https://doi.org/10.1016/j.physe.2018.02.007.

[30] O. H. Laguna, A. Pérez, M. A. Centeno, and J. A. Odriozola, "Synergy Between Gold and Oxygen Vacancies in Gold Supported on Zr-Doped Ceria Catalysts for the CO Oxidation," *Applied Catalysis B: Environmental* 176-177 (2015): 385–395, https://doi.org/10.1016/j.apcatb.2015.04.019.

[31] K. S. Kumar and N. V. Jaya, "Synthesis and Characterization of Pure and Sn-Doped CeO 2 Nanoparticles," *Asian Journal of Chemistry* 25, no. 11 (2013): 6095–6098, https://doi.org/10.14233/ajchem.2013.14267.

[32] M. Aslam, F. Fozia, A. Gul, et al., "Phyto-Extract-Mediated Synthesis of Silver Nanoparticles Using Aqueous Extract of *Sanvitalia procumbens*, and Characterization, Optimization and Photocatalytic Degradation of Azo Dyes Orange G and Direct Blue-15," *Molecules* 26, no. 20 (2021): 6144, https://doi.org/10.3390/molecules26206144.

[33] Y. Rashid, I. Ahmad, I. Ahmad, N. Ahmad, M. Aslam, and A. Alotaibi, "Affective Antidepressant, Cytotoxic Activities, and Characterization of Phyto-Assisted Zinc Oxide Nanoparticles Synthesized Using *Sanvitalia procumbens* Aqueous Extract," *BioMed Research International* 2022 (2022): 1–10, https://doi.org/10.1155/2022/1621372.

[34] A. Arumugam, C. Karthikeyan, A. S. Haja Hameed, K. Gopinath, S. Gowri, and V. Karthika, "Synthesis of Cerium Oxide Nanoparticles Using *Gloriosa superba L.* Leaf Extract

and Their Structural, Optical and Antibacterial Properties," *Materials Science and Engineering: C* 49 (2015): 408–415, https://doi.org/10.1016/j.msec.2015.01.042.

[35] J. K. Sharma, P. Srivastava, S. Ameen, M. S. Akhtar, S. K. Sengupta, and G. Singh, "Phytoconstituents Assisted Green Synthesis of Cerium Oxide Nanoparticles for Thermal Decomposition and Dye Remediation," *Materials Research Bulletin* 91 (2017): 98–107, https://doi.org/10.1016/j.materresbull.2017.03.034.

[36] N. Pandiyan, B. Murugesan, J. Sonamuthu, S. Samayanan, and S. Mahalingam, "Facile Biological Synthetic Strategy to Morphologically Aligned CeO_2/ZrO_2 Core Nanoparticles Using Justicia Adhatoda Extract and Ionic Liquid: Enhancement of its Bio-Medical Properties," *Journal of Photochemistry and Photobiology B: Biology* 178 (2018): 481–488, https://doi.org/10.1016/j.jphotobiol.2017.11.036.

[37] Z. Chen, Y. Ding, N. Fang, and C. Liu, "Fabrication and Photocatalytic Activities of Dark Brown CeO2 With a Crystalline-Core/Disordered-Shell Heterostructure," *Materials Research Express* 5, no. 6 (2018): 065905, https://doi.org/10.1088/2053-1591/aac801.

[38] M. Singh, M. Goyal, and K. Devlal, "Size and Shape Effects on the Band Gap of Semiconductor Compound Nanomaterials," *Journal of Taibah University for Science* 12, no. 4 (2018): 470–475, https://doi.org/10.1080/16583655.2018.1473946.

[39] J. Malleshappa, H. Nagabhushana, B. D. Prasad, S. C. Sharma, Y. S. Vidya, and K. S. Anantharaju, "Structural, Photoluminescence and Thermoluminescence Properties of CeO2 Nanoparticles," *Optik* 127, no. 2 (2016): 855–861, https://doi.org/10.1016/j.ijleo.2015.10.114.

[40] S. R. Ali, R. Kumar, A. Kalam, A. G. Al-Sehemi, and M. C. Arya, "Effect of Strontium Doping on the Band Gap of CeO_2 Nanoparticles Synthesized Using Facile Co-Precipitation," *Arabian Journal for Science and Engineering* 44, no. 7 (2019): 6295–6302, https://doi.org/10.1007/s13369-018-03700-x.

[41] S. A. Ansari, M. M. Khan, M. O. Ansari, S. Kalathil, J. Lee, and M. H. Cho, "Band Gap Engineering of CeO2 Nanostructure Using an Electrochemically Active Biofilm for Visible Light Applications," *RSC Advances* 4, no. 32 (2014): 16782–16791, https://doi.org/10.1039/c4ra00861h.

[42] H. Ghaznavi, R. Najafi, S. Mehrzadi, et al., "Neuro-Protective Effects of Cerium and Yttrium Oxide Nanoparticles on High Glucose-Induced Oxidative Stress and Apoptosis in Undifferentiated PC12 Cells," *Neurological Research* 37, no. 7 (2015): 624–632, https://doi.org/10.1179/1743132815y.0000000037.

[43] K. Govindarasu, K. Gnanasekaran, S. Balaraman, et al., "Study on Enhanced Antibacterial and Cytotoxicity of Pure and Cadmium Doped Cerium Oxide Against Gram-Positive and Gram-Negative Bacteria," *Soft Nanoscience Letters* 09, no. 01 (2019): 1–16, https://doi.org/10.4236/snl.2019.91001.

[44] S. Erachikkaiah, S. Sreenivasa, H. S. Lalithamba, D. Suresh, P. C. Nethravathi, and K. P. Sharath, "Synthesis, Characterization of Zr Doped and Zr/Sr-Dual Doped Ceo2 Nanoparticles With Their Photocatalytic and Cytotoxic Activities," *Characterization of Zr Doped and Zr/Sr-Dual Doped Ceo2 Nanoparticles With Their Photocatalytic and Cytotoxic Activities* (2024).

[45] A. Lateef, B. I. Folarin, S. M. Oladejo, P. O. Akinola, L. S. Beukes, and E. B. Gueguim-Kana, "Characterization, Antimicrobial, Antioxidant, and Anticoagulant Activities of Silver Nanoparticles Synthesized From *Petiveria alliacea L.* Leaf Extract," *Preparative Biochemistry & Biotechnology* 48, no. 7 (2018): 646–652, https://doi.org/10.1080/10826068.2018.1479864.

[46] S. Mathad, S. Mathad, S. Malladi, et al., "Sol–Gel Co-Precipitation Synthesis, Anticoagulant and Anti-Platelet Activities of Copper-Doped Nickel Manganite Nanoparticles," *Gels* 7, no. 4 (2021): 269, https://doi.org/10.3390/gels7040269.

[47] E. Fuentes, B. Yameen, C. Salvador-Morales, I. Palomo, and C. Vilos, "Antiplatelet Effect of Differentially Charged PEGylated Lipid-Polymer Nanoparticles," *Nanomedicine: Nanotechnology, Biology and Medicine* 13, no. 3 (2017): 1089–1094, https://doi.org/10.1016/j.nano.2016.10.010.